Nuclear Engineering and Technology 52 (2020) 51–58

Contents lists available at ScienceDirect

Nuclear Engineering and Technology

journal homepage: www.elsevier.com/locate/net

Original Article

Preliminary analysis and design of the heat exchangers for the Molten Salt Fast Reactor

Andrea Di Ronco, Antonio Cammi*, Stefano Lorenzi

Politecnico di Milano, Department of Energy, via La Masa 34, 20156, Milano, Italy

ARTICLE INFO

Article history:
Received 28 January 2019
Received in revised form
14 June 2019
Accepted 11 July 2019
Available online 19 July 2019

Keywords:
Molten salt reactor
MSFR
Heat exchanger
Printed circuit heat exchanger
Gen-IV

ABSTRACT

Despite the recent growth of interest in molten salt reactor technology and the crucial role which heat transfer plays in the design of power reactors, specific studies on the design of heat exchangers for the Molten Salt Fast Reactor have not yet been performed. In this work we deliver a preliminary but quantitative analysis of the intermediate heat exchangers, based on reference design data from the SAMOFAR H2020-Euratom project. Two different promising reference technologies are selected for study thanks to their compactness features, the Printed Circuit and the Helical Coil heat exchangers. We present preliminary design results for each technology, based on simplified design tools. Results highlight the limiting effects of the compactness constraints imposed on the fuel salt inventory and the allowed size. Large pressure drops on both flow sides are to be expected, with negative consequences on pumping power and natural circulation capabilities. The small size required for the flow channels also represents possible fabrication issues and safety concerns regarding channel blockage.

1. Introduction

The Molten Salt Fast Reactor (MSFR) is a further development of the graphite moderated molten salt breeder reactor originally designed at the Oak Ridge National Laboratory (ORNL) in the 1960's [1], and is the current reference design studied within the framework of the Generation IV International Forum [2]. Despite the general renewal of interest in molten-salt-fuelled reactors, the studies on the MSFR that are found in literature focus mainly on neutronics, core dynamics and thermal-hydraulics, materials, and fuel cycle analysis [3]. Even though the heat exchangers and the intermediate loop play a crucial role in the design of a power reactor, specific studies have not yet been performed. In particular, the MSFR design requires a strong compactness (and hence high heat transfer rate) of the heat exchangers in order to limit the fuel salt in non-active region. To this aim, classic heat exchangers cannot fulfil this goal, calling for new innovative heat exchanger design. Among them, the Printed Circuit Heat Exchanger (PCHE), the Plate Heat Exchanger (PHE) and the Helical Coil Heat Exchanger (HCHE) seem the most promising and they have been also selected for other Generation-IV systems. For example [4], conducted an extensive computational study on different types of Printed Circuit Heat Exchangers (PCHE) with application to sodium-cooled reactors (SFR) and gas-cooled reactors (HTGR). In Ref. [5] PCHEs were studied for molten salt-SCO_2 applications in the Fluoride salt-cooled High-temperature Reactor (FHR). A comparison of different compact heat exchanger designs for helium-helium applications in a generic 600 MW high temperature reactor was performed in Ref. [6]. A comprehensive computational analysis was done in Ref. [7] to derive friction factor correlations in HCHEs for sodium applications. Speaking in terms of power density, however, the requirements dictated by the MSFR design here considered are much more severe than in other applications such as gas-cooled reactors (e.g. the VHTR). Other designs such as SFRs are more comparable to the MSFR in terms of power density, but differ substantially on compactness requirements grounds due to the pool-type design and the allowed volume for the primary circuit.

This work aims at performing a preliminary but quantitative analysis of aspects which are relevant to the design of the MSFR plant, focusing on the intermediate heat exchangers (IHX) and providing possible useful information for the selection of the MSFR design option for the IHX. In this framework, two different reference technologies are considered, due to their compactness features. Given the preliminary phase of the design process, the investigation of fabricability issue as well as blockage problem are out of the scope of this paper. In Section 3, the design of intermediate heat exchangers (Fig. 1, in red) is addressed. The compactness of the primary circuit, as prescribed by the current design of the

* Corresponding author.
E-mail address: antonio.cammi@polimi.it (A. Cammi).

https://doi.org/10.1016/j.net.2019.07.013

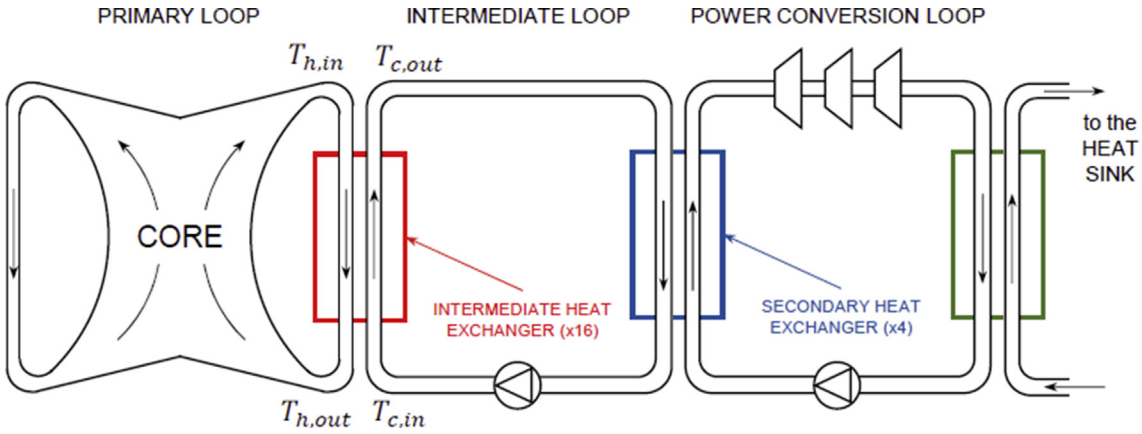

Fig. 1. Simplified scheme of the Molten Salt Fast Reactor plant.

MSFR, has important consequences on the design of the heat exchangers, imposing severe constraints on size and on the allowable fuel salt inventory. We present a simplified design approach for both and discuss the resulting designs.

2. Reference design of the Molten Salt Fast Reactor

The MSFR is conceived, at the current design stage, as a large-size nuclear reactor for commercial power production. Its total thermal power output is intended to be around 3000 MW_{th}, with a net electrical power output in the 1000–1500 MW_{el} range, depending on the achievable plant conversion efficiency. The employment of a liquid fuel allows a low fuel inventory and a high power density, resulting in a very compact reactor geometry [8]. The reference MSFR data adopted in this work is the one proposed in the framework of the SAMOFAR (Safety Assessment of the Molten Salt Fast Reactor) project (http://samofar.eu/). Despite the extensive studies carried out on the reactor core, many design options are still to be investigated and defined.

The primary and intermediate loop temperatures, which are of fundamental importance for the design of the intermediate heat exchangers, are not yet defined. The fuel salt temperature at core inlet and outlet are expected to be in the 650–700 °C and 750–800 °C ranges, respectively. Assuming a 100 °C core temperature rise, we selected 675 °C and 775 °C as guess values for this work. In this preliminary analysis, the choice is to consider the intermediate temperatures as additional design variables for the intermediate heat exchangers and to present design results covering broad temperature ranges.

Additional constraints are required by design. If the total fuel salt volume is set to 18 m^3 and 50% of it is supposed to be within the core [9], the maximum fuel salt volume available for each intermediate heat exchanger will be somewhat lower than 0.56 m^3. A reasonable assumption could be 0.35 m^3, considering the volumes required by piping and pumps. Furthermore, issues related to the erosion of structural materials impose a limit on the maximum salt velocity everywhere within. the primary and intermediate loops (5 m/s) [10]. The main design parameters discussed so far and their adopted values are listed in Table 1 (nomenclature for temperatures is chosen in consistency with the intermediate heat exchangers viewpoint).

Table 1
Main reference design parameters and constraints.

Quantity	Unit	Value
Core power output	MW	3000
Number of primary loop sectors	–	16
Int. heat exch. heat transfer rate	MW	187.5
Core outlet temperature, $T_{h,in}$	°C	775
Core inlet temperature, $T_{h,out}$	°C	675
Int. loop maximum temperature, $T_{c,out}$	°C	variable
Int. loop minimum temperature, $T_{c,in}$	°C	variable
Max. fuel salt inventory (per heat exch.)	m^3	0.35
Maximum salt velocity	m s^{-1}	5

Two main options are considered for the choice of the fuel salt composition [11,12]. The first one is LiF–ThF_4–$^{233}UF_4$, whereas the second one is LiF–ThF_4–$^{235}UF_4$-(Pu-MA)F_3. The first one has not yet been characterised and, in general, properties of these salts depend on the exact composition (which might vary during the design process). For these reasons, for the present analysis the properties of the blanket salt LiF–ThF_4 (77.5–22.5 %mol) are used. Its properties have been extensively investigated and are taken from Refs. [13,14].

Regarding the intermediate salt, several options are considered by the SAMOFAR project. They are all fluoride salts and their properties are in general quite similar. Two options are selected for this work, the FLiNaK and FLiBe salts. Their compositions are LiF-NaF-KF (46.5–11.5-42 %mol) and LiF–BeF_2 (66-34 %mol), respectively. Their properties are taken from Ref. [15].

3. Intermediate heat exchanger analysis

The large power density and the compact layout of the MSFR result in a small allowable size for the intermediate heat exchangers, complicating the extraction of the heat from the reactor core. A properly designed heat exchanger should feature an optimal combination of large heat transfer surfaces, large temperature differences and efficient heat transfer mechanisms. Given a thermal power amount such as the one of the MSFR, with such severe size constraints, heat extraction is a demanding task from the design, manufacturing and operation viewpoints. In particular, large pressure drops might be expected, with significant consequences on operation and safety (e.g. requiring a large pumping power and hindering natural circulation capabilities).

The allowable size is fundamental for the design of the intermediate heat exchangers, but currently no precise constraints from the designers are given. The numerical values adopted in the following are therefore tentative, but still consistent with the preliminary design of the reactor core:

- L = 2.50 m
- W = 1.50 m
- H = 1.00 m

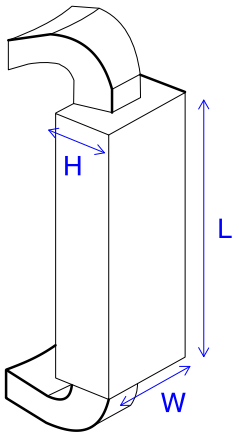

Fig. 2. Allowable dimensions for the intermediate heat exchangers.

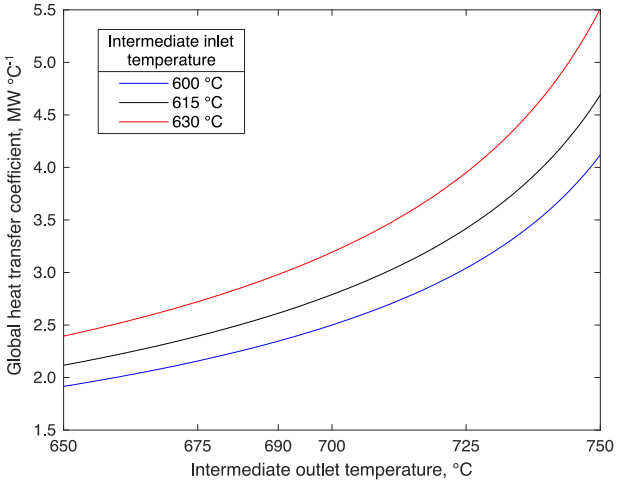

Fig. 3. Required global heat transfer coefficient UA, as a function of $T_{c,in}$ and $T_{c,out}$.

Each of the 16 intermediate heat exchangers is contained in the volume defined by the three dimensions L, W, and H, as shown in Fig. 2.

3.1. Candidate technologies

Several criteria should be considered for the selection of candidate technologies for the MSFR intermediate heat exchangers:

- Compact size
- Resistance to high temperatures, up to 750–800 °C
- Low salt inventory
- Low pressure drops

The severe constraints prescribed by the reactor design, together with the high temperatures and the employment of unconventional fluids such as molten salts, pose demanding technological challenges, so that established heat exchanger technologies suitable for molten salt applications are hard to identify. Here, two different technologies are considered:

1. Printed Circuit Heat Exchanger (PCHE)
2. Helical Coil Heat Exchanger (HCHE)

The PCHE is a relatively new technology, developed and manufactured by Heatric (https://www.heatric.com). Their unique manufacturing technique is called "diffusion bonding" and consists in an innovative solid-state process [16]. Printed circuit heat exchangers are new to the nuclear industry, but might represent a promising solution due to their resistance to high temperatures and their compactness. Possible points of weakness can be constituted by the creep/fatigue damages and fabricability issues for the specific MSFR case. On the other hand, the HCHE technology is well-established in the nuclear field and offers better performance than in the case of more conventional shell-and-tube heat exchangers [17].

3.2. Modelling assumptions

The solution of the general heat exchange problem can be complicated so that detailed, reliable results can only be obtained by numerical simulation associated with experimental validation. Nevertheless, analytical solutions can still be obtained for simple geometries and boundary conditions, providing mathematical tools that are useful for a preliminary design. We make the following modelling assumptions:

i. the fluids exchange heat in counterflow;
ii. the external heat exchanger boundaries are adiabatic;
iii. axial heat conduction along the channels is neglected;
iv. potential and kinetic energy changes are neglected;
v. fluid properties are constant with temperature and equal to average values;
vi. the overall heat transfer coefficient is constant;
vii. internal heat generation in the fuel salt is neglected.

The global performance of the heat exchanger is assessed by means of the $\varepsilon - NTU$ method [18]:

$$NTU(\varepsilon, C_r) = \frac{1}{C_r - 1}\log\left(\frac{\varepsilon - 1}{C_r\varepsilon - 1}\right) \tag{1}$$

where

$$C_r = \frac{C_{min}}{C_{max}} \tag{2}$$

$$\varepsilon = \frac{C_h(T_{h,in} - T_{h,out})}{C_{min}(T_{h,in} - T_{c,in})} \tag{3}$$

$$NTU = \frac{UA}{C_{min}} \tag{4}$$

For the definition of temperature levels please refer to Fig. 1. From (1)it is evident that the global heat transfer coefficient UA increases monotonically with the heat exchanger effectiveness ε, meaning that a heat exchanger which is supposed to reach a high effectiveness must provide a large heat transfer surface. Required values of UA for different values of $T_{c,in}$ and $T_{c,out}$ are depicted in Fig. 3. For given values of the operating temperatures, the required UA is computed from (1). The heat exchanger is then designed by means of simplified models, which allow to relate UA to a small set of design parameters.

3.3. Printed circuit heat exchanger

The simplified geometric scheme of the PCHE adopted for the analysis is shown in Fig. 4. The chosen design parameter is the channel diameter d_{ch}. The other geometrical parameters appearing in Fig. 4 are simply assumed proportional to d_{ch}:

$$t_p = 1.25\,\frac{d_{ch}}{2} \tag{5}$$

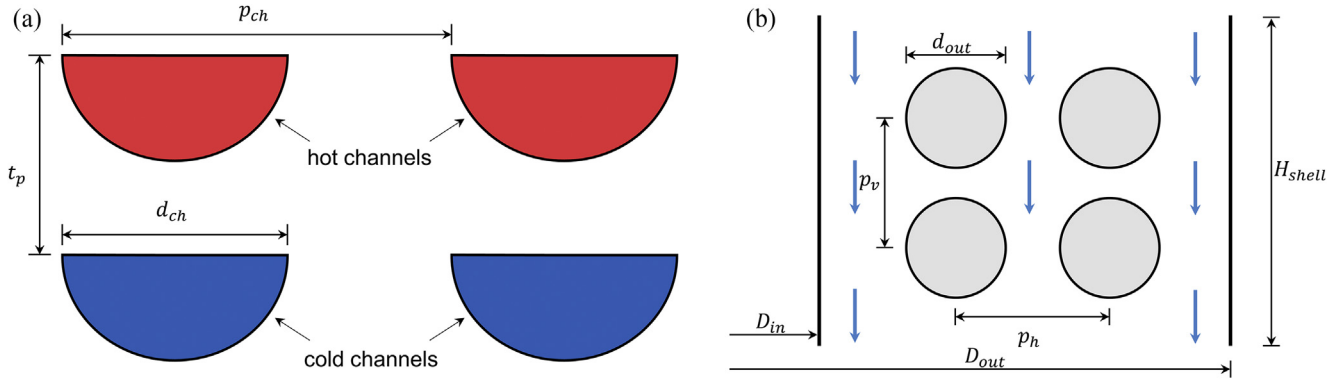

Fig. 4. (a) PCHE geometry, (b) HCHE geometry.

$$p_{ch} = 1.25\, d_{ch} \tag{6}$$

With reference to Fig. 2, the length of the channels is set equal to L, while the other dimensions of the heat exchanger are assumed equal to W and H. The number of channels (per side) n_{ch} is therefore determined by d_{ch} and by the heat exchanger dimensions. The total heat transfer area and the overall heat transfer coefficient are computed as

$$A = L\left(d_{ch} + \pi\frac{d_{ch}}{2}\right)n_{ch} \tag{7}$$

$$U = \left(\frac{1}{h_h} + \frac{t_p}{k_w} + \frac{1}{h_c}\right)^{-1} \tag{8}$$

where the average hot side and cold side heat transfer coefficients, h_h and h_c, are given by correlations for fully developed laminar flows in semi-circular ducts [19]:

$$Nu_i = \frac{h_i D_H}{k_i} = 4.089, \qquad (i = h, c) \tag{9}$$

where Nu_i are the Nusselt numbers and k_i are the thermal conductivities of the fluids. The distributed pressure drops are given by

$$\Delta p_h = 2\, f_h\, \rho_h\, u_h^2 \frac{L}{D_H} \tag{10}$$

$$\Delta p_c = 2\, f_c\, \rho_c\, u_c^2 \frac{L}{D_H} \tag{11}$$

where the average Fanning friction factors f_h and f_c are taken from Ref. [19]:

$$f_i = \frac{15.767}{Re_i} \tag{12}$$

with Re_ibeing the Reynolds numbers.

3.4. Helical coil heat exchanger

The model is based on the simplified geometry depicted in Fig. 4. The horizontal and vertical pitch p_h and p_v are supposed proportional to the outer diameter of the tubes d_{out}:

$$p_h = p_v = 1.25\, d_{out} \tag{13}$$

The tube thickness t_t is set to a relatively low value (0.3 mm), since no inner/outer pressure difference occurs. Following the same approach adopted for the design of the heat exchangers for the MSRE, the hotter fuel salt is placed in the shell side [1].

As shown in Fig. 4, the tubes are arranged in radial (i.e. horizontal) rows, whose number N_{rows} is maximised given d_{out} and the shell dimensions. The shell inner diameter D_{in} is fixed to 0.20 m, while the outer one D_{out} is fixed by the heat exchanger dimension H. The number of turns of the tubes is maximised, to deliver the largest possible heat transfer surface. Regarding the total number of the tubes, it is computed as the minimum multiple of N_{rows} required to set the maximum salt velocity in the tubes below the 5 m/s constraint. The velocities in the tube rows are iteratively solved by imposing the total mass flow rate and a uniform pressure drop. The number of tube headers, here fixed to 8 (4 at inlet, 4 at the outlet), is also considered. The iterative design procedure can be outlined as follows:

1. For each value of the tube inner diameter d_{in}, the other dependent geometrical parameters (d_{out}, p_h, p_v, N_{rows}) are computed accordingly to the contraints.
2. The number of turns is maximised, taking into account the tube diameter and vertical pitch, the shell height and the number of headers N_{head} (i.e. it must be the highest possible multiple of 1/N_{head}).
3. Since for each row both the friction factor and the length are different, the mass flow rate is redistributed among the tube rows in order to obtain a uniform pressure drop distribution.
4. The process is iterated by increasing the total number of tubes until the highest tube velocity falls below the 5 m/s constraint.

Pressure drops and average heat transfer coefficients are estimated by means of proper correlations. Regarding the tube side, the Ito correlation for single-phase turbulent flow Darcy friction factor [20],

$$f_{Ito} = 0.304\, Re_{tube}^{-0.25} + 0.029\left(\frac{D_{coil}}{d_{in}}\right)^{-0.5} \tag{14}$$

and the ESDU correlation for single-phase turbulent heat transfer in coiled pipes [21] are adopted. The shell side friction factor and heat transfer coefficient are obtained by using the correlations provided by Žukauskas for aligned tube banks [18,22]. The overall heat transfer coefficient is computed for the i-th row and then averaged:

$$U_{shell,i} = \left[\frac{1}{h_{shell}} + \frac{d_{out}}{2t_t}\ln\left(\frac{d_{out}}{d_{in}}\right)\frac{t_t}{k_w} + \left(\frac{d_{out}}{d_{in}}\right)\frac{1}{h_{tube,i}}\right]^{-1} \tag{15}$$

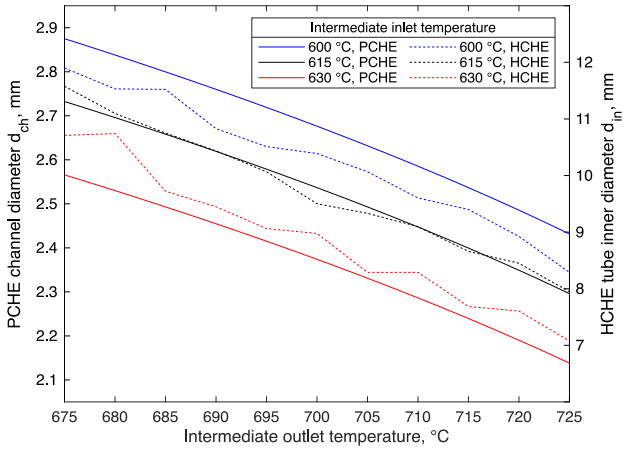

Fig. 5. Resulting values of the design parameters d_{ch} and d_{in} as functions of $T_{c,in}$ and $T_{c,out}$.

$$\overline{U}_{shell} = \frac{\sum_i U_{shell,i}\, L_{tube,i}}{\sum_i L_{tube,i}} \tag{16}$$

$$UA = \overline{U}_{shell}\, N\, \pi d_{out} \sum_i L_{tube,i} \tag{17}$$

4. Design results and discussion

The simplified models briefly described in the previous sections allow the design of the heat exchanger given a single geometrical design parameter d, namely d_{ch} for the PCHE and d_{in} for the HCHE. It is therefore possible to obtain, at least approximately, the design parameter value $\overline{d}$which satisfies

$$UA(\overline{d}, \boldsymbol{\lambda}) = UA_{req}(\boldsymbol{\lambda}) \tag{18}$$

where $\boldsymbol{\lambda}$ represents the other main design parameters, namely $T_{c,in}$ and $T_{c,out}$, while UA_{req} is given by (1)-(4). We selected three possible values of $T_{c,in}$(600 °C, 615 °C, 630 °C), which are sufficiently high to ensure proper margins with respect to the freezing point of typical fuel salts [14]. Regarding $T_{c,out}$, we considered several values between 675 °C and 725 °C. The following results, obtained by means of (18), are valid for the FLiNaK case. The results for the FLiBe case, which are analogous to the presented ones, are here omitted for brevity. The resulting values of d_{ch} and d_{in} are shown in Fig. 5. It is evident that, as also shown in Fig. 3, an increase in $T_{c,in}$ and $T_{c,out}$ leads to smaller temperature differences between the two fluids and to larger heat transfer surfaces, requiring more and smaller

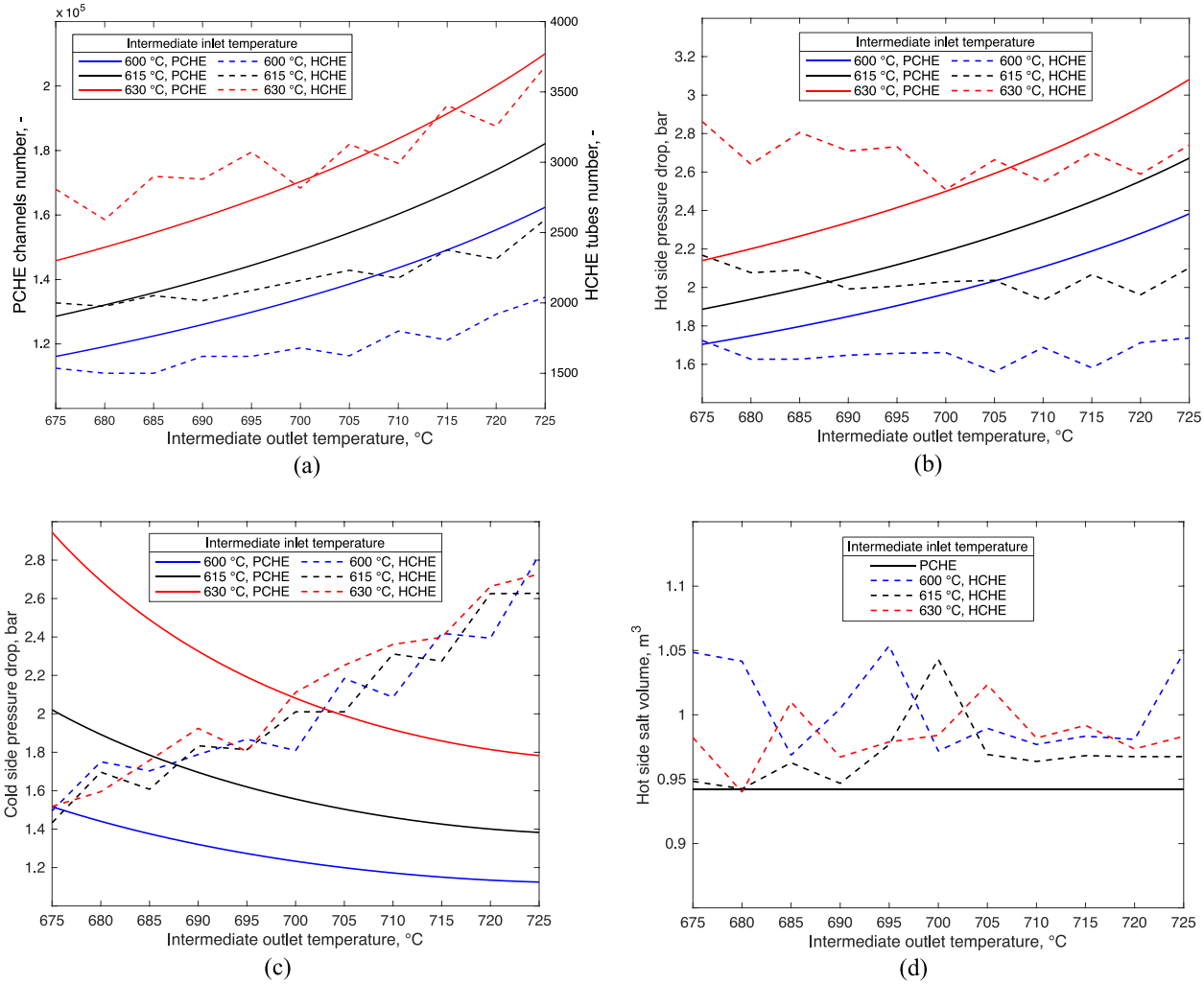

Fig. 6. (a) Number of channels/tubes, (b) hot side distributed pressure drop, (c) cold side distributed pressure drop and (d) fuel salt inventory of the intermediate heat exchangers for the resulting design parameters, as functions of $T_{c,in}$ and $T_{c,out}$.

channels/tubes (Fig. 6a). This effect is more evident for the PCHE, since the small size of the channels limits the Reynolds numbers to the laminar flow regime and the heat exchange requirements must be fulfilled by the heat transfer surface alone. The HCHE operates in the turbulent flow regime due to the higher Reynolds numbers and to the properties of coiled tubes, hence variations in the nominal mass flow rates (due to different temperature conditions) affect the heat transfer mechanisms as well. This justifies the adoption of larger flow channels and higher salt velocities. The temperature values considered cover a rather broad range of possible nominal operating conditions, showing that the adoption of the PCHE or HCHE technologies would imply flow channel sizes of the order of 2–3 mm or 7–12 mm, respectively. These are very low values, posing severe issues from the design, manufacturing, operation and safety viewpoints. The risks associated with channel blockage might be critical in view of the fissile content and of the high freezing point of the fuel salt, especially for the PCHE case.

The effects of the constraints imposed on heat exchanger dimensions are also evident from the analysis of the pressure drops and of the fuel salt inventory. Pressure drops in the hot side (Fig. 6b) and cold side (Fig. 6c) reach both relatively high values (of the order of 1–3 bar, for distributed pressure drops alone), with relevant consequences on the required pumping power and on natural circulation capabilities of the MSFR. Fig. 6d shows that the operating temperatures have small (HCHE) or virtually no (PCHE) influence on the fuel salt inventory, suggesting a strict relation with the heat exchanger size itself. The parametric analysis highlights mainly two aspects:

- the small channel diameter required for the PCHE and HCHE in order to fulfil the volume salt constraint and consequently the difficulty in reaching configuration with low salt inventory
- the non-negligible pressure drops in the HX that may have relevant consequences on the required pumping power and on natural circulation capabilities of the MSFR

The first aspect seems unavoidable especially for the nature of the PCHE that impose channels of the order of mm (ranging from 1.5 to 3 mm). The difficulty in reaching the low salt inventory design constrain can be overcome lowering the lowest temperature in the intermediate circuit which calls for a lower required heat transfer coefficient. As a drawback, this results in reducing the margin to the primary side solidification.

Only for PCHE, the pressure drop can be limited considering the possibility to act on the W and H size. At constant fuel salt volume, an increase in the space available in radial direction (i.e., increasing width or height of the heat exchanger) turns out in a reduction of the length and in a reduction of the velocity, both having a positive impact on the pressure drop. Doubling the product W*H leads to a reduction of the pressure drops by a factor of 4. To this aim, in Table 2, the comparison of two possible PCHE design is provided, considering H = 1.5 m (Option 1) and H = 2 m (Option 2).

The curves in Fig. 5 and 6 show non-continuous trends for the resulting designs for the HCHE, as opposed to the PCHE. This behaviour is a consequence of the discrete design procedure adopted for the HCHE (see Section 3.4). In the PCHE case, the channel diameter is allowed to vary in an approximately continuous way on the basis of a very simple geometry. For the HCHE, the more complex geometrical relationships between the tube size, the number of turns, the number of headers, the number of rows and, ultimately, the constraints on the overall size of the heat exchanger act in a discrete way. The design procedure aims at optimizing a single parameter, i.e., the tube diameter, to deliver a prescribed UA, leading to non-continuous, possibly non-monotonic results. In some cases, trends can be clearly observed despite the non-continuous behaviour, as in Fig. 5 and in Fig. 6a–c. In the other cases, trends are not observed and results suggest, for the HCHE, the hot side pressure drop and salt volume being not sensitive with respect to the intermediate outlet temperature. Nevertheless, over the considered range of temperatures, the comparison between the two technologies shows similar results even when the trends are different. For completeness, we summarise in Table 3 the geometrical parameters of the optimised HCHE configurations for each considered value of $T_{c,in}$ and $T_{c,out}$.

5. Conclusion

The performed analysis resulted in a preliminary design of the intermediate heat exchangers for the Molten Salt Fast Reactor. Both the considered technologies, the printed circuit and the helical coil heat exchangers, proved to be capable of transferring the reactor core power output to the intermediate loop while satisfying most of the reactor design constraints identified in the framework of the SAMOFAR project. Hypotheses were made mainly on the intermediate loop temperatures, in order to find a trade-off between the highest possible temperature differences in the heat exchangers and a safety margin to avoid the solidification of the fuel salt.

Among all the constraints and prescriptions, the maximum allowed size and fuel salt inventory have proven to be the most restrictive ones. The compactness requirements prescribed by the core design lead to very tight geometries and to small flow cross sections in the heat exchangers. The main effect is that pressure drops are expected to be large, with important consequences on the required pumping power and on the possibility of taking advantage of natural circulation. As for the PCHE, the salt inventory constraint can be respected only using tiny channel (less than 2 mm) and imposing 600 °C as lower temperature for the intermediate heat exchanger. The pressure drop, in this case, ranges from 1.6 to 1 bar if

Table 2
PCHE design for option 1 (H = 1.5 m) and option 2 (H = 2 m).

Parameter	Symbol	Unit	Option 1		Option 2	
			FliNaK	FLiBe	FliNaK	FLiBe
Intermediate circuit higher temp.	$T_{c,out}$	°C	670	670	670	670
Intermediate circuit lower temp.	$T_{c,in}$	°C	600	600	600	600
Width	W	m	1	1	1	1
Height	H	m	1.5	1.5	2	2
Length	L	m	0.96	1.06	0.79	0.962
Channel diameter	d_{ch}	mm	1.8	1.9	2	1.8
Plate thickness	t_p	mm	1.1	1.2	1.3	1.1
Channels number	n_{ch}	–	295704	265651	320000	394272
Hot channel pressure drop	Δp_h	bar	1.67	1.49	0.84	1.26
Cold channel pressure drop	Δp_c	bar	1.61	2.83	1.59	0.69
Fuel salt volume	V_{salt}	m^3	0.360	0.398	0.398	0.483

Table 3
Summary of HCHE optimised geometrical parameters and properties for $T_{c,in}$ = 600 °C, 615 °C and 630 °C.

$T_{c,in}$ = 600 °C									
$T_{c,out}$ (°C)	d_{in} (mm)	$p_v = p_h$ (mm)	N_{tubes}	N_{rows}	N	N_{head}	Δp_{shell} (bar)	Δp_{tubes} (bar)	V_{salt} (m^3)
675	11.9	15.6	1536	24	64	4	1.72	1.50	1.048
680	11.5	15.2	1500	25	60	4	1.63	1.75	1.042
685	11.5	15.2	1500	25	60	4	1.63	1.70	0.969
690	10.8	14.3	1620	27	60	4	1.65	1.79	1.005
695	10.5	13.9	1620	27	60	4	1.66	1.87	1.054
700	10.4	13.7	1680	28	60	4	1.66	1.81	0.972
705	10.1	13.3	1624	29	56	4	1.56	2.18	0.990
710	9.6	12.8	1800	30	60	4	1.69	2.09	0.977
715	9.4	12.5	1736	31	56	4	1.58	2.42	0.983
720	8.9	11.9	1920	32	60	4	1.71	2.39	0.981
725	8.3	11.1	2040	34	60	4	1.74	2.83	1.048
$T_{c,in}$ = 615 °C									
$T_{c,out}$ (°C)	d_{in} (mm)	$p_v = p_h$ (mm)	N_{tubes}	N_{rows}	N	N_{head}	Δp_{shell} (bar)	Δp_{tubes} (bar)	V_{salt} (m^3)
675	11.6	15.2	2000	25	80	4	2.17	1.43	0.948
680	11.1	14.2	1976	26	76	4	2.08	1.70	0.942
685	10.8	14.2	2052	27	76	4	2.09	1.61	0.963
690	10.4	13.8	2016	28	72	4	1.99	1.83	0.947
695	10.1	13.3	2088	29	72	4	2.01	1.81	0.977
700	9.5	12.6	2160	30	72	4	2.03	2.01	1.043
705	9.3	12.4	2232	31	72	4	2.04	2.01	0.969
710	9.1	12.1	2176	32	68	4	1.93	2.31	0.964
715	8.7	11.6	2376	33	72	4	2.07	2.27	0.968
720	8.4	11.3	2312	34	68	4	1.96	2.63	0.967
725	7.4	10.7	2592	36	72	4	2.10	2.63	0.967
$T_{c,in}$ = 630 °C									
$T_{c,out}$ (°C)	d_{in} (mm)	$p_v = p_h$ (mm)	N_{tubes}	N_{rows}	N	N_{head}	Δp_{shell} (bar)	Δp_{tubes} (bar)	V_{salt} (m^3)
675	10.7	14.1	2808	27	104	4	2.86	1.52	0.983
680	10.7	14.1	2592	27	96	4	2.64	1.59	0.940
685	9.7	12.9	2900	29	100	4	2.81	1.76	1.010
690	9.4	12.6	2880	30	96	4	2.71	1.92	0.967
695	9.1	12.1	3072	32	96	4	2.73	1.81	0.979
700	9.0	12.0	2816	32	88	4	2.51	2.11	0.984
705	8.3	11.1	3128	34	92	4	2.66	2.25	1.023
710	8.3	11.1	2992	34	88	4	2.55	2.36	0.982
715	7.7	10.4	3404	37	92	4	2.70	2.40	0.992
720	7.6	10.3	3256	37	88	4	2.59	2.66	0.973
725	7.1	9.6	3680	40	92	4	2.74	2.73	0.983

a wider space is available in the HX section. As the selection of the intermediate salt, it turns out that the FLiBe can be preferred for the reduction of the volume salt inventory. On the other hand, the use of FLiNaK may reduce the pressure drop on the intermediate side. As for the HCHE, the inventory constraint can be respected with very small tube and outer shell diameter (6/5 mm and 0.7 m, respectively) but this design leads to unbearable pressure drop on the fuel salt side. With more relaxed constraints (tube diameter ~ 10 mm, outer shell diameter 1 m), the HCHE has lower pressure drop (2 bar) but a greater fuel salt volume (~1 m^3).

Finally, it must be emphasized that the technological feasibility of such compact heat exchangers for molten salt applications needs further investigation. Besides the already mentioned problematics related to large pressure losses, fabrication could represent a severe limitation. Channel blockage may also be a relevant issue especially for printed circuit heat exchangers, if channels are supposed to be so small. Furthermore, creep/fatigue behaviour of such critical components has not been examined so far.

Disclaimer

The content of this paper does not reflect the official opinion of the European Union. Responsibility for the information and/or views expressed therein lies entirely with the authors.

Acknowledgments

This project has received funding from the EURATOM research and training programme 2014–2018 under grant agreement No 661891.

Abbreviations

FHR	Fluoride salt-cooled High-temperature Reactor
FLiBe	$LiF–BeF_2$ mixture (66-34 %mol)
FLiNaK	LiF-NaF-KF mixture (46.5–11.5-42 %mol)
HCHE	Helical Coil Heat Exchanger
HTGR	High Temperature Gas Reactor
HX	heat exchanger
IHX	intermediate heat exchanger
MSFR	Molten Salt Fast Reactor
MSRE	Molten-Salt Reactor Experiment
ORNL	Oak Ridge National Laboratory
PCHE	Printed Circuit Heat Exchanger
PHE	Plate Circuit Heat Exchanger
SAMOFAR	Safety Assessment of the Molten Salt Fast Reactor
SCO_2	supercritical CO_2
SFR	Sodium-cooled Fast Reactor
VHTR	Very-High-Temperature Reactor

Nomenclature

A	total PCHE heat transfer area, m^2
C_c	heat capacity rate of the cold side fluid, W/°C
C_h	heat capacity rate of the hot side fluid, W/°C
C_{max}	maximum between $C_h$and C_c, W/°C
C_{min}	minimum between $C_h$and C_c, W/°C
C_r	C_{min}/C_{max} ratio
d	geometric design parameter
$\overline{d}$	optimal geometric design parameter
d_{ch}	diameter of PCHE channels, mm
D_{coil}	diameter of HCHE tube coils, m
D_H	equivalent hydraulic diameter, mm
d_{in}	inner diameter of HCHE tubes, mm
D_{in}	inner diameter of HCHE shell, m
d_{out}	outer diameter of HCHE tubes, mm
D_{out}	outer diameter of HCHE shell, m
f_c	average Fanning friction factor of PCHE cold side fluid
f_h	average Fanning friction factor of PCHE hot side fluid
f_{Ito}	Ito correlation Darcy friction factor
h_c	average PCHE cold side heat transfer coefficient, W/m^2 °C
h_h	average PCHE hot side heat transfer coefficient, W/m^2 °C
h_{shell}	average heat transfer coefficient of HCHE shell side fluid, W/m^2 °C
$h_{tube,i}$	heat transfer coefficient of HCHE tube side fluid (i-th row), W/m^2 °C
k_c	thermal conductivity of PCHE cold side fluid, W/m °C
k_h	thermal conductivity of PCHE hot side fluid, W/m °C
k_w	heat exchanger metal thermal conductivity, W/m °C
L	W, Hallowed dimensions of the heat exchanger, m
$L_{tube,i}$	length of HCHE tubes (i-th row), m
N	number of HCHE tubes per tube row
n_{ch}	number of PCHE channels (per side)
N_{head}	number of HCHE flow headers
N_{rows}	number of HCHE tube rows
NTU	number of transfer units of the heat exchanger
Nu_c	average Nusselt number of PCHE cold side fluid
Nu_h	average Nusselt number of PCHE hot side fluid
p_{ch}	pitch of PCHE channels, mm
p_h	horizontal pitch of HCHE tubes, mm
p_v	vertical pitch of HCHE tubes, mm
Re_c	Reynolds number of PCHE cold side fluid
Re_h	Reynolds number of PCHE hot side fluid
Re_{tube}	Reynolds number of HCHE tube side fluid
$T_{c,in}$	intermediate loop minimum temperature, °C
$T_{c,out}$	intermediate loop maximum temperature, °C
$T_{h,in}$	core outlet temperature, °C
$T_{h,out}$	core inlet temperature, °C
t_p	thickness of PCHE plates, mm
t_t	thickness of HCHE tubes, mm
U	overall PCHE heat transfer coefficient, W/m^2 °C
UA	global heat transfer coefficient, W/°C
UA_{req}	objective global heat transfer coefficient, W/°C
u_c	average velocity of PCHE cold side fluid, m/s
u_h	average velocity of PCHE hot side fluid, m/s
$U_{shell,i}$	overall HCHE shell side heat transfer coefficient (i-th row), W/m^2 °C
$\overline{U}_{shell}$	overall HCHE shell side heat transfer coefficient (average), W/m^2 °C
V_{salt}	Volume of fuel salt inside a heat exchanger, m^3

Greek symbols

Δp_c	distributed pressure drop of PCHE cold side, bar
Δp_h	distributed pressure drop of PCHE hot side, bar
ε	effectiveness of the heat exchanger
λ	non-geometric design parameters ($T_{c,in}$ and $T_{c,out}$)
ρ_c	density of PCHE cold side fluid, kg/m^3
ρ_h	density of PCHE hot side fluid, kg/m^3

Appendix A. Supplementary data

Supplementary data to this article can be found online at https://doi.org/10.1016/j.net.2019.07.013.

References

[1] P.N. Haubenreich, J.R. Engel, Experience with the molten-salt reactor experiment, Nucl. Appl. Technol. 8 (1970) 118–136, https://doi.org/10.13182/NT8-2-118.

[2] Generation IV International Forum 2016 Annual Report, 2016. https://www.gen-4.org/gif/upload/docs/application/pdf/2017-07/gifannual_report_2016_final12july.pdf.

[3] J. Serp, M. Allibert, O. Beneš, S. Delpech, O. Feynberg, V. Ghetta, D. Heuer, D. Holcomb, V. Ignatiev, J.L. Kloosterman, L. Luzzi, E. Merle-Lucotte, J. Uhlíř, R. Yoshioka, D. Zhimin, The molten salt reactor (MSR) in generation IV: overview and perspectives, Prog. Nucl. Energy 77 (2014) 308–319, https://doi.org/10.1016/J.PNUCENE.2014.02.014.

[4] S.H. Yoon, H.C. NO, G.B. Kang, Assessment of straight, zigzag, S-shape, and airfoil PCHEs for intermediate heat exchangers of HTGRs and SFRs, Nucl. Eng. Des. 270 (2014) 334–343, https://doi.org/10.1016/J.NUCENGDES.2014.01.006.

[5] I.H. Kim, X. Zhang, R. Christensen, X. Sun, Design study and cost assessment of straight, zigzag, S-shape, and OSF PCHEs for a FLiNaK–SCO2 Secondary Heat Exchanger in FHRs, Ann. Nucl. Energy 94 (2016) 129–137, https://doi.org/10.1016/J.ANUCENE.2016.02.031.

[6] N. Bartel, M. Chen, V.P. Utgikar, X. Sun, I.-H. Kim, R. Christensen, P. Sabharwall, Comparative analysis of compact heat exchangers for application as the intermediate heat exchanger for advanced nuclear reactors, Ann. Nucl. Energy 81 (2015) 143–149, https://doi.org/10.1016/J.ANUCENE.2015.03.029.

[7] D.A. Haskins, M.S. El-Genk, CFD analyses and correlation of pressure losses on the shell-side of concentric, helically-coiled tubes heat exchangers, Nucl. Eng. Des. 305 (2016) 531–546, https://doi.org/10.1016/J.NUCENGDES.2016.05.014.

[8] D. Heuer, E. Merle-Lucotte, M. Allibert, M. Brovchenko, V. Ghetta, P. Rubiolo, Towards the thorium fuel cycle with molten salt fast reactors, Ann. Nucl. Energy 64 (2014) 421–429, https://doi.org/10.1016/j.anucene.2013.08.002.

[9] H. Rouch, O. Geoffroy, P. Rubiolo, A. Laureau, M. Brovchenko, D. Heuer, E. Merle-Lucotte, Preliminary thermal–hydraulic core design of the molten salt fast reactor (MSFR), Ann. Nucl. Energy 64 (2014) 449–456, https://doi.org/10.1016/J.ANUCENE.2013.09.012.

[10] C. Fiorina, The Molten Salt Fast Reactor as a Fast-Spectrum Candidate for Thorium Implementation, Politecnico di Milano, 2013.

[11] D. Gerardin, M. Allibert, D. Heuer, A. Laureau, E. Merle-Lucotte, C. Seuvre, Design evolutions of molten salt fast reactor, in: Int. Conf. Fast React. Relat. Fuel Cycles Next Gener. Nucl. Syst. Sustain. Dev. Yekaterinburg, Russ. June 26-29, 2017.

[12] M. Tano, P. Rubiolo, O. Doche, Progress in modeling solidification in molten salt coolants, Model. Simul. Mater. Sci. Eng. 25 (2017) 074001, https://doi.org/10.1088/1361-651X/aa8345.

[13] M. Brovchenko, E. Merle, H. Rouch, F. Alcaro, M. Allibert, M. Aufiero, A. Cammi, S. Dulla, O. Feynberg, L. Frima, O. Geoffroy, V. Ghetta, D. Heuer, V. Ignatiev, J.L. Kloosterman, D. Lathouwers, A. Laureau, L. Luzzi, B. Merk, P. Ravetto, A. Rineiski, P. Rubiolo, L. Rui, M. Szieberth, S. Wang, B. Yamaji, Optimization of the Pre-conceptual Design of the MSFR, 2014.

[14] V. Ignatiev, O. Feynberg, A. Merzlyakov, A. Surenkov, A. Zagnitko, Progress in Development of MOSART Concept with Th Support, 2012, pp. 943–952.

[15] O. Beneš, R.J.M. Konings, Molten salt reactor fuel and coolant, in: Compr. Nucl. Mater., 2012, pp. 359–389, https://doi.org/10.1016/B978-0-08-056033-5.00062-8.

[16] D. Southall, R. Le Pierres, S.J. Dewson, Design Considerations for Compact Heat Exchangers, Icapp '08., 2008, pp. 1953–1968.

[17] L. Santini, A. Cioncolini, M.T. Butel, M.E. Ricotti, Flow boiling heat transfer in a helically coiled steam generator for nuclear power applications, Int. J. Heat Mass Transf. 92 (2016) 91–99, https://doi.org/10.1016/j.ijheatmasstransfer.2015.08.012.

[18] F.P. Incropera, D.P. DeWitt, T.L. Bergman, A.S. Lavine, Fundamentals of Heat and Mass Transfer, 2007, https://doi.org/10.1016/j.applthermaleng.2011.03.022.

[19] M.A. Ebadian, Z.F. Dong, Forced convection, internal flow in ducts, in: Y.I.C.W.M. Rohsenow, J.P. Hartnett (Eds.), Handb. Heat Transf., 1998, pp. 5.1–5.137.

[20] H. Ito, Friction factors for turbulent flow in curved pipes, J. Basic Eng. 81 (1959) 123–134.

[21] ESDU 78031: Internal Forced Convective Heat Transfer in Coiled Pipes, 2001. https://www.esdu.com/cgi-bin/ps.pl?sess=unlicensed_1180605073308jgz&t=doc&p=esdu_78031b. (Accessed 5 June 2018).

[22] A.A. Zukauskas, Heat transfer from tubes in cross flow, Adv. Heat Transf. Acad. Press. 8 (1972) 93–106, https://doi.org/10.1016/S0065-2717(08)70038-8.